Effects of time, temperature, and steel composition on growth and dissolution of inclusions in liquid steels

T. Hong and T. DebRoy

The current knowledge of stability and growth/dissolution kinetics of inclusions in liquid steels is synthesised to understand their growth and dissolution behaviour. In particular, it is shown that the effects of time and temperature on the diffusion controlled growth and dissolution behaviour of inclusions can be represented by a set of time–temperature–transformation (TTT) diagrams. The TTT diagrams for the growth of oxide, nitride, and sulphide inclusions show the characteristic C shape, with each plot having an optimal temperature where the highest growth rate is achieved. The inclusion dissolution rate depends strongly on the initial inclusion radius and temperature. Apart from the stability of various inclusions in a given composition of steel, the diagrams provide important kinetic information for diffusion controlled growth and dissolution of oxide, nitride, and sulphide inclusions. I&S/1570

The authors are in the Department of Materials Science and Engineering, Pennsylvania State University, University Park, PA 16802, USA (debroy@psu.edu). Manuscript received 24 October 2000; accepted 27 June 2001.

INTRODUCTION

Oxide, sulphide, and nitride inclusions are frequently present in steels. Since the safety and reliability of welded steel structures are affected by the composition, number density, and size distribution of inclusions,[1,2] many of the recent investigations on inclusions have focused on the steel weld metal. Much of the data on inclusion stability that were generated from decades of research on ladle deoxidation have been useful in recent investigations of inclusion stability during welding. For example, Kluken and Grong[3] studied the precipitate stability, volume fraction, size, and chemical composition of inclusions from weld metal chemistry in Al–Ti–Si–Mn steel welds. Frost and Brothers[4] studied the sequence of oxide formation during solidification of the weld pool by considering the effects of microsegregation of oxygen and deoxidants in the liquid metal. Bhadeshia and Svensson[5] predicted inclusion composition as a function of weld metal composition and a precipitation sequence based on thermodynamics. These studies together with computer applications of thermodynamics in complex systems have led to significant improvements in understanding the behaviour of inclusions in weld metals. For instance, Hsieh *et al.*[6] used the ThermoCalc™ software to predict the sequence of inclusion formation in low alloy steel welds by considering equilibrium thermodynamics.

Apart from the thermodynamic investigations, the rates of growth and/or dissolution of inclusions have received considerable attention. For example, Goto *et al.*[7] showed that the cooling rate influences the inclusion growth rate significantly. Ratke and Thieringer[8] showed that the motion of the particles accelerates the kinetics of coarsening and broadens the normalised inclusion size distribution. Babu *et al.*[9,10] calculated the rate of precipitation of the oxide inclusions from the diffusion rate of elements to the inclusion/liquid metal interface. Christian[11] presented theories of diffusional and interface controlled growth of precipitates. Whelan[12] proposed a method to calculate the rate of diffusion controlled dissolution of spherical precipitates.

Recent investigations have led to significant advances in the nature of the inclusions in welded steel metal through characterisation[13,14] and better understanding of the stability and rates of dissolution and growth of inclusions. By contrast, synthesis of these component processes to gain a comprehensive understanding of the growth and dissolution behaviour of the inclusions has been mostly overlooked. Many examples in the literature demonstrate the importance of such synthesis. For example, current theories of heat treatment of steels are based on the well accepted time–temperature–transformation (TTT) diagrams that synthesise both the kinetics and the thermodynamics of phase transformations. Hong and DebRoy[15] recently proposed a formalism to understand the effects of time and temperature on the growth and dissolution of inclusions based on thermodynamics and kinetics. In this paper, the authors extend this concept to construct a set of TTT diagrams that describe the effects of time and temperature on the growth and dissolution behaviour of inclusions in steels of known compositions. The effects of alloy composition on the growth and dissolution rates of oxide, nitride, and sulphide inclusions are investigated at various temperatures.

Modelling procedure

The construction of the TTT diagrams requires the consideration of growth and dissolution rates of inclusions. The diffusional growth and dissolution rates depend on the element diffusion rates near the inclusion/alloy interface. These diffusion rates depend on the difference between the concentrations of various species in the bulk alloy and interface. Therefore, the calculation of the interfacial concentrations of the constituent elements of the inclusions is a prerequisite for the calculations. To simplify calculations of the rates of growth and dissolution of inclusions in liquid steels, the following assumptions were made.

1. The concentration field near each inclusion was assumed to be constant during the nucleation, growth, or dissolution of inclusions.

2. The activities of liquid iron and all solid compounds were assumed to be unity.

3. At the interface between the inclusion and the liquid steel, only the concentrations of those elements that constitute the inclusion were calculated. The concentrations of all other elements were assumed to be the same as those in the bulk metal.

4. The growth and dissolution of inclusions were assumed to be controlled by the diffusion of constituent elements in liquid steels. The diffusion coefficients used are presented in Table 1. Because of the lack of availability of the diffusion

 ISSN 0301-9233

Table 1 Alloy composition and diffusion coefficient of oxygen in calculations[3,16,17]

Element	Composition 1, wt-%	Composition 2, wt-%	D, $m^2 s^{-1}$
C	0·09	0·06	$7{\cdot}2\times10^{-9}$
Si	0·53	0·39	$3{\cdot}6\times10^{-9}$
Mn	1·9	1·55	$4{\cdot}1\times10^{-9}$
Ni	0·09	0·2	...
Cr	0·01	0·01	...
Ti	0·005	0·003	$7{\cdot}4\times10^{-9}$
Al	0·010	0·016	$8{\cdot}3\times10^{-9}$
N	0·008	0·004	$3{\cdot}7\times10^{-9}$
O	0·032	0·054	$9{\cdot}2\times10^{-9}$
S	0·020	0·009	$4{\cdot}8\times10^{-9}$

coefficient data at high temperatures, some of the data presented in this table are extrapolated from low temperature values.

5. The nucleation rates of inclusions are high as shown in the Appendix and the incubation time is short compared with the growth time. Therefore, the nucleation phenomenon is ignored in the calculations.

Equilibrium concentrations at interface

For a known alloy composition and temperature, the interfacial concentrations can be calculated assuming equilibrium of inclusion formation reaction at the interface between the inclusion and the liquid steel. The reaction is expressed by

$$xM + yO \rightleftharpoons M_xQ_y \qquad (1)$$

where M is a metallic element such as Al, Ni, Mn, Si, or Ti, and Q denotes a deoxidant element such as O, N, or S. The equilibrium constant for the reaction is given by

$$k_{eq} = \frac{a_{M_xQ_y}}{a_M^x a_Q^y} = \frac{1}{[f_M c_M^i]^x [f_Q c_Q^i]^y} = \exp\left(-\frac{\Delta G^0}{RT}\right) \qquad (2)$$

where $a_{M_xQ_y}$, a_M, and a_Q are the activities of M_xQ_y, M, and Q; c_M^i and c_Q^i are the interfacial concentrations (in weight per cent) of M and Q; ΔG^0 is the standard free energy change for the reaction (1); and f_M and f_Q are the activity coefficients of M and Q given by

$$f_i = 10^{\sum_{j=1}^{n} e_i^j c_j^i} \qquad (3)$$

where e_i^j is the first order interaction parameter between element i and j, c_j^i is the concentration of element j at the interface, and n is the number of elements considered in the alloy. The values of ΔG^0 for all reactions considered are presented in Table 2. Considering the diffusion fluxes of M and Q to or from the interface, the following equation can be derived[20]

$$c_M^i = c_M^b - \frac{x m_M}{y m_Q}\left(\frac{D_Q}{D_M}\right)^{1/2}(c_Q^b - c_Q^i) \qquad (4)$$

where c_M^b and c_Q^b are the concentrations (in weight per cent) of M and Q in the bulk metal, m_M and m_Q are the atomic weights of M and Q, and D_M and D_Q are the diffusion coefficients of M and Q in liquid steel. The interfacial concentrations of M and Q, c_M^i and c_Q^i, can be obtained from the solution of equations (2) and (4). After calculating the interfacial concentrations, a variable c^* is defined as the dimensionless supersaturation of the element with a lower diffusion coefficient in the alloy[11]

$$c^* = (c^b - c^i)/(c^p - c^i) \qquad (5)$$

where c^p is the concentration (in weight per cent) of the element that has lower diffusivity in the alloy.

TTT diagrams for growth

When the interfacial concentrations of M and Q are lower than their concentrations in the bulk liquid, the elements diffuse from the bulk liquid toward the interface and the inclusions experience growth. The increase in the radius of the inclusions is calculated using equation (6)[13]

$$r_{i+1} - r_i = \frac{\alpha}{2(t)^{1/2}}\Delta t_i \qquad (6)$$

where r_i and r_{i+1} are the radii of the inclusion before and after the ith time step, respectively, Δt_i is the time step, t is time, and α is a growth rate parameter expressed by[11]

$$\alpha = (2Dc^*)^{1/2} \qquad (7)$$

where D is the diffusion coefficient of the element with lower diffusivity in liquid steel, given by

$$D = D^0 \exp\left(-\frac{E}{RT}\right) \qquad (8)$$

where D^0 is a temperature independent pre-exponential term and E is the activation energy for diffusion. The time necessary to increase the inclusion radius to a certain value at different temperatures is calculated from equation (6) to construct the TTT diagrams for the growth of inclusions.

TTT diagrams for dissolution

When the interfacial concentrations of constituent elements of the inclusion exceed the concentrations in the bulk liquid at a given temperature, the elements diffuse from the interface into the bulk liquid and the inclusions experience dissolution. By considering diffusion controlled precipitation with a quasi-steady state approximation in the alloy matrix, Whelan[12] derived the following expression for the kinetics of dissolution

$$r_{i+1} - r_i = -\frac{k}{2}\left[\frac{D}{r_i} + \left(\frac{D}{\pi t}\right)^{1/2}\right]\Delta t_i \qquad (9)$$

where r_i and r_{i+1} are the radii of the inclusion before and after the ith time step Δt_i, respectively, t is the dissolution time of the inclusion, and $k = -2c^*$. The time needed to decrease the particle size to a certain value can be calculated from equation (9) to construct the TTT diagrams for the dissolution of inclusions.

Results and discussion

Figure 1 shows the calculated nucleation rate of Al_2O_3 inclusions using a procedure described in the Appendix. It is observed from the computed results that the nucleation rate is very high. Therefore, it is reasonable to assume that the nucleation rate is high compared with the growth and dissolution rates. For this reason, the nucleation phenomenon was not considered in the calculations reported in this paper.

Table 2 Standard free energy for various reactions:[18,19] $\Delta G^o = a + bT$, cal mol^{-1} (1 J ≡ 4·184 cal)

Precipitation reaction	a	b
$2\underline{Al} + 3\underline{O} = Al_2O_3$	−289 060	93·52
$3\underline{Ti} + 5\underline{O} = Ti_3O_5$	−419 680	136·5
$\underline{Ti} + 2\underline{O} = TiO_2$	−161 460	55·95
$\underline{Si} + 2\underline{O} = SiO_2$	−140 950	54·62
$\underline{Mn} + \underline{O} = MnO$	−68 816	29·95
$\underline{Al} + \underline{N} = AlN(s)$	−134 000	46·5
$3\underline{Si} + 4\underline{N} = Si_3N_4$	−203 000	75·3
$\underline{Ti} + \underline{N} = TiN$	−80 380	24·29
$\underline{Fe} + \underline{S} = FeS$	−111 370	57·0
$\underline{Mn} + 2\underline{Al} + 4\underline{O} = MoO.Al_2O_3$	−369 376	125·22
$\underline{Si} + 2\underline{Al} + 5\underline{O} = SiO_2.Al_2O_3$	−319 875	97·32
$\underline{Mn} + \underline{Si} + 4\underline{O} = MnN.SiO_2$	−200 466	75·0

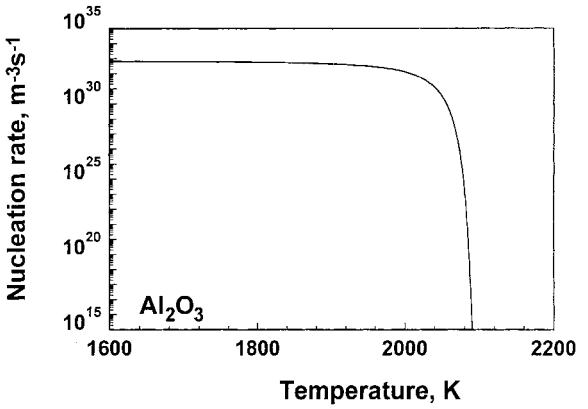

1 Nucleation rate of Al_2O_3 inclusions versus temperature in liquid steel of composition 1 (*see* Table 1)

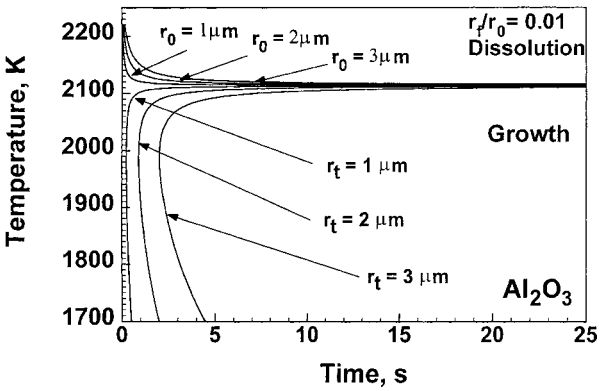

2 TTT diagrams for growth and dissolution of Al_2O_3 inclusions with different radi in liquid steel of composition 1

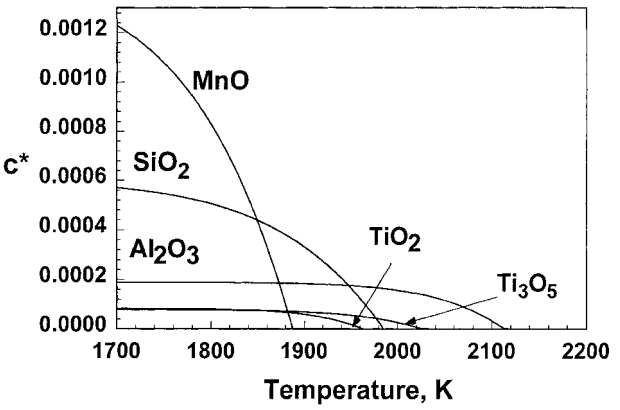

3 Change of dimensionless supersaturation of oxygen c^* for several oxide inclusions with temperature for steel of composition 1

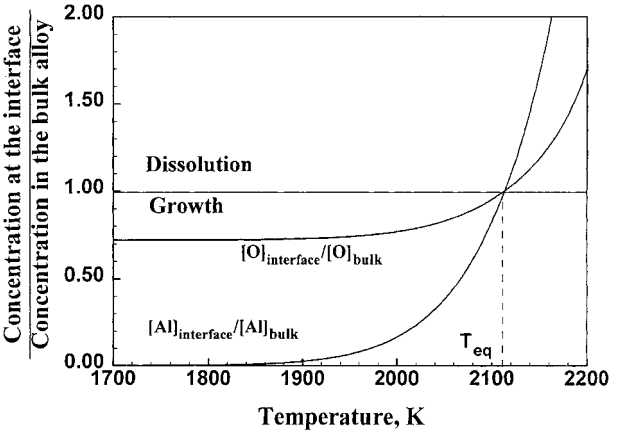

4 Equilibrium concentrations of aluminium and oxygen at the interface of Al_2O_3 inclusions and liquid alloy at different temperatures in steel of composition 1

Figure 2 shows the TTT diagram for the growth and dissolution of Al_2O_3 inclusions for the steel of composition 1 indicated in Table 1. For growth, the plots indicate the time necessary for inclusions to reach various target radii ($r_t = 1$, 2, and 3 μm in this plot) at various temperatures during isothermal growth. The plots for dissolution indicate the time necessary for inclusions to reach the final radius r_f (1% of r_0 in this figure) from various initial radii ($r_0 = 1$, 2, and 3 μm in this plot).

The growth rates of inclusions depend on the diffusion coefficient D and the concentration difference represented by the dimensionless concentration c^*. The diffusion coefficient in the liquid metal, calculated from equation (8), decreases with reduction of temperature. However, the dimensionless concentration c^* increases with decrease in temperature, as observed in Fig. 3. As a result, there is an optimal value of temperature at which the highest growth rate is achieved. The resulting TTT diagrams for the growth of Al_2O_3 inclusions show the typical C shape curve.

Both oxygen and aluminium diffuse from the bulk melt to the inclusion/melt interface during growth of Al_2O_3. The direction of transport is reversed during dissolution. The concentrations of oxygen and aluminium at the interface and in the bulk liquid determine the growth and dissolution rates of the inclusions. These concentrations vary with temperature for a given steel composition. The dimensionless interfacial concentrations of oxygen and aluminium at different temperatures are shown in Fig. 4 for an alumina inclusion in a steel of composition 1 to illustrate this behaviour. Growth of alumina stops at a temperature when the interfacial concentrations of oxygen and aluminium become equal to those in the bulk alloy. For the steel composition used in this calculation, the concentrations of both oxygen and aluminium at the interface and in the bulk steel become equal at 2114 K. This temperature is defined as the equilibrium temperature for the alumina inclusion–steel system. The alumina inclusions will grow in the liquid steel below this temperature and dissolve above this temperature.

Figure 5 shows the TTT diagrams for the growth of various oxide inclusions to 1 μm radius in a liquid steel of composition 1. Of all the oxide inclusions considered, Al_2O_3, $MnO.Al_2O_3$, and Ti_3O_5 grow fastest at temperatures above 2000 K. It is observed from Fig. 3 that the change of c^* at lower temperatures is not very pronounced for Al_2O_3, Ti_3O_5, and TiO_2. As a result, the change of diffusion coefficient dominates the kinetics of inclusion growth. For

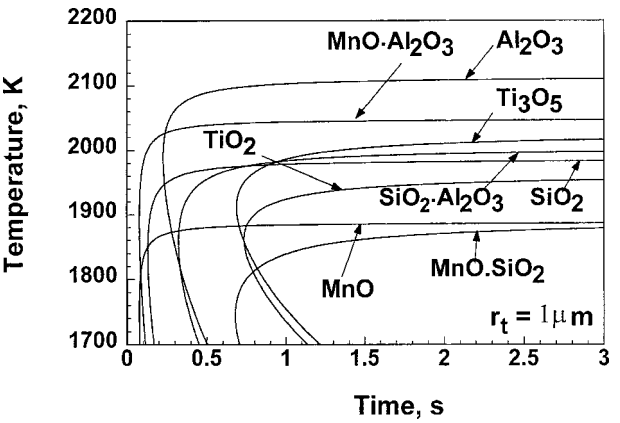

5 TTT diagrams for growth of various oxide inclusions in liquid steel of composition 1

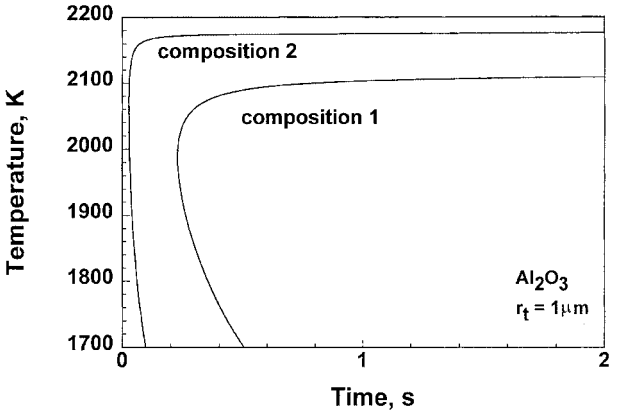

6 Comparison of growth rates of Al_2O_3 inclusions between composition 1 and composition 2

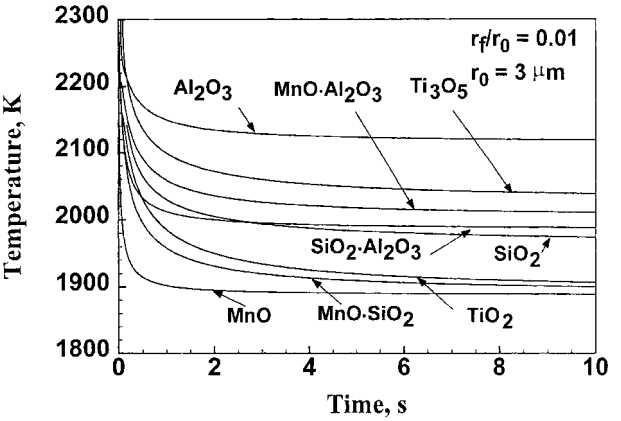

8 TTT diagrams for dissolution of all oxide inclusions considered in liquid alloy of composition 1

MnO and SiO_2, the change of c^* with reduction in temperature exceeds the corresponding change of diffusion coefficient and the change in concentration c^* dominate the kinetics of inclusion growth. Therefore, the C curve shapes of TTT diagrams for growth of MnO and SiO_2 are not as pronounced as for the other inclusions. It is observed from Fig. 5 that the equilibrium temperatures of the complex oxides considered in this paper are intermediate between the equilibrium temperatures of the constituent simple oxides. For example, the equilibrium temperature $MnO.Al_2O_3$ lies between those of Al_2O_3 and MnO. A similar behaviour is observed for both $SiO_2.Al_2O_3$ and $MnO.SiO_2$ inclusions.

To investigate the influence of alloy composition on the growth kinetics, Fig. 6 shows the comparison between the kinetics of Al_2O_3 inclusion growth in liquid steels of compositions 1 and 2. The growth rate of Al_2O_3 inclusions for composition 2 is much higher than that for composition 1. This phenomenon can be explained from the calculated values of dimensionless supersaturation c^* in these two cases (Fig. 7). It is observed that c^* for alloy 2 is much higher than for alloy 1. It can be derived from equations (5) and (6) that the growth rate increases with the increase of c^*. Therefore, the growth kinetics for alloy 2 is faster than for alloy 1. Figure 8 shows the computed TTT diagrams for the dissolution of oxide inclusions of different initial radii for the composition 1. It indicates the time necessary to reduce the radii of inclusions from their original size r_0 to r_f (1% of r_0 in this plot) at different temperatures. The dissolution kinetics depends strongly on time and temperature, as can be observed.

It is observed from Figs. 5 and 8 that there is an equilibrium temperature between the inclusions and steel above which the inclusions experience dissolution. The higher the equilibrium temperature of an inclusion, the higher its stability. Several researchers presented theoretical and experimental results on the relative stability of inclusions in low alloy steels. For example, Hsieh *et al.*[6] calculated the sequence of oxidation. Their result showed that the sequence depended on the composition and temperature. Of the oxides they considered, Al_2O_3, Ti_3O_5, and $MnO.Al_2O_3$ were calculated to be most stable at higher temperatures in the low alloy steels. These relative stability values agree well with the computed results in Fig. 7. However, their[6] calculations did not consider some complex oxides. Dowling *et al.*[21] studied the inclusions in submerged arc welds in low alloy steels using transmission electron microscopy and EDS. They found that $MnO.Al_2O_3$, a titanium rich compound, and an aluminium rich phase (probably Al_2O_3) were the main constituents. Kluken and Grong[3] studied inclusion formation in Al–Ti–Si–Mn deoxidised steel welds. The calculated stability of various oxides decreases in the following order: Al_2O_3, Ti_2O_3, SiO_2, MnO. The high stability of Al_2O_3, $MnO.Al_2O_3$, and Ti_3O_5 observed by these investigators is consistent with the computed TTT diagrams presented in Figs. 5 and 8.

Figures 9 and 10 shows the TTT diagrams for the growth and dissolution of several nitride and sulphide inclusions, respectively. It is observed that the equilibrium temperatures for the stability of FeS, Si_3N_4, MnS, and TiN inclusions are much lower than for the corresponding metal oxides. Other features of these plots are similar to those for the oxide inclusions. Because of their low equilibrium temperatures, the sulphide inclusions cannot form in the low alloy steel weld pool where the temperatures are higher than the equilibrium temperature for these inclusions. However, they can form during solidification of the weld metal. From

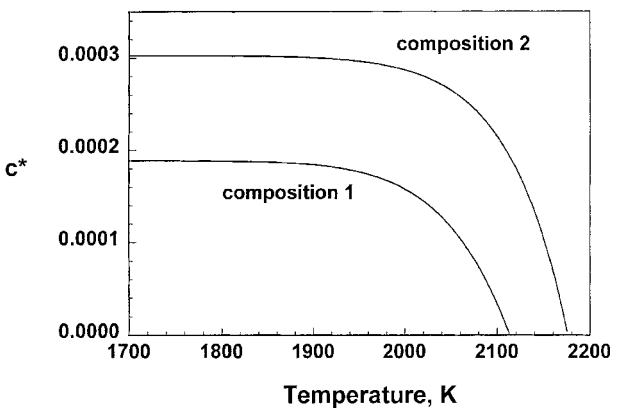

7 Comparison of dimensionless supersaturation of oxygen c^* at interface of Al_2O_3 inclusions and liquid steels of compositions 1 and 2

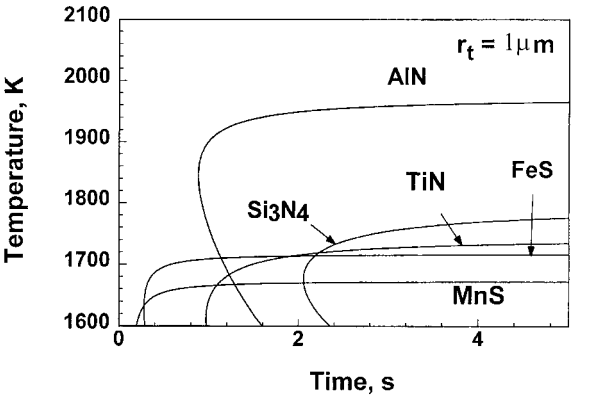

9 TTT diagrams for growth of several nitride and sulphide inclusions in liquid alloy

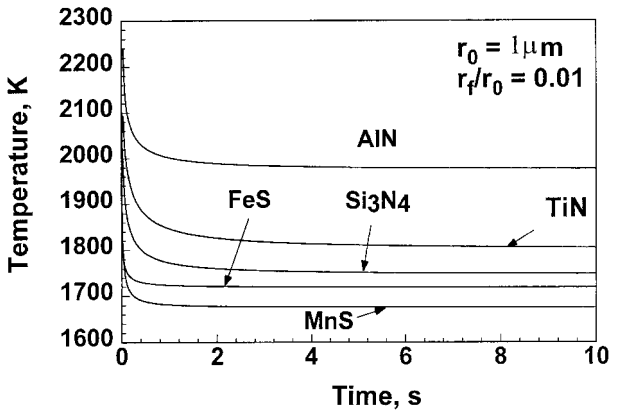

10 TTT diagrams for dissolution of several nitride and sulphide inclusions in liquid alloy of composition 1

Fig. 9, it is observed that, although the equilibrium temperature of MnS is lower than that of FeS, its growth rate at low temperatures is higher, which implies that MnS may become the dominant inclusion during solidification and cooling. This conclusion from theoretical calculations matches experimental observations well in the sense that MnS is known to be the dominant sulphide inclusion in many steels.[22,23]

CONCLUSIONS

The diffusion controlled growth and dissolution behaviour of oxide, nitride, and sulphide inclusions can be represented by a serious of time–temperature–transformation (TTT) diagrams that indicate the strong effects of time and temperature on the kinetics of their growth and dissolution. In the low alloy steel investigated, Al_2O_3, $MnO.Al_2O_3$, and Ti_3O_5 are the most stable inclusions that form during welding. Some complex oxide inclusions such as $SiO_2.Al_2O_3$ are also stable at high temperatures. The composition of steel has a strong effect on the TTT diagrams of the inclusions. Apart from the stability of various inclusions in a given composition of steel, the diagrams provide important kinetic information of diffusion controlled growth and dissolution.

ACKNOWLEDGEMENTS

The present study was supported by the Division of Materials Sciences, Office of Basic Energy Sciences, the US Department of Energy under the grant DE-FG02-84ER45158. The authors thank Dr S. S. Babu for helpful discussions.

APPENDIX

Nucleation rate of inclusions

The homogeneous nucleation rate of inclusions in the liquid steel I_v is given by[10]

$$I_v = A \exp\left\{\frac{-\Delta G^*_{hom}}{KT}\right\} = A \exp\left\{-\frac{16\pi\sigma^3 V_m^2}{3kT\Delta G^2}\right\} \qquad (10)$$

where A is a constant[10] equal to $10^{33}\ m^{-3}\ s^{-1}$, ΔG^*_{hom} is the activation energy for the formation of the nucleus, ΔG is the free energy change for reaction (1) described in the text above and calculated using the data in Table 2, V_m is the molar volume of the inclusion calculated from the density and the molecular weight of the inclusions, σ is the interfacial energy of the inclusion[10] taken as $0{\cdot}5\ J\ m^{-2}$, and k is Boltzmann's constant. As observed in Fig. 1, the calculated homogeneous nucleation rate is very high. If the nucleation rate was calculated considering heterogeneous nucleation, the nucleation rate would be higher than the rates presented in Fig. 1. The incubation time of nucleation calculated from the nucleation rate[13] is of the order of 10^{-8}–10^{-4} s. This incubation time is much shorter than the time necessary for the growth of inclusions presented in this paper.

REFERENCES

1. D. J. ABSON: *Weld. World*, 1989, **27**, 76–101.
2. E. S. KAYALI, J. M. CORBETT, and H. W. KERR: *J. Mater. Sci. Lett.*, 1983, **2**, 123–128.
3. O. KLUKEN and O. GRONG: *Metall. Trans.*, 1989, **20A**, 1335–1349.
4. G. FROST and D. G. BROTHERS: *Scr. Metall. Mater.*, 1995, **32**, 1061–1066.
5. H. K. D. H. BHADESHIA and L. E. SVENSSON: 'Mathematical modelling of weld phenomena', (ed. H. Cerjak and K. E. Easterling), 109–180; 1993, London, The Institute of Materials.
6. K. C. HSIEH, S. S. BABU, J. M. VITEK, and S. A. DAVID: *Mater. Sci. Eng.*, 1996, **A215**, 84–91.
7. H. GOTO, K. MIYAZAWA, W. YAMADA, and K. TANAKA: *ISIJ Int.*, 1995, **35**, 708–714K.
8. L. RATKE and W. K. THIERINGER: *Acta Metall.*, 1985, **33**, 1793–1802.
9. S. S. BABU, S. A. DAVID, J. M. VITEK, K. MUNDRA, and T. DEBROY: *Mater. Sci. Technol.*, 1995, **11**, 186–199.
10. S. S. BABU, S. A. DAVID, J. M. VITEK, K. MUNDRA, and T. DEBROY: in Proc. 4th Int. Conf. 'Trends in welding research', Gatlinburg, TN, 1998.
11. J. W. CHRISTIAN: 'The theory of transformations in metals and alloys – Part 1: Equilibrium and general kinetic theory', 2nd edn; 1981, Oxford, Pergamon Press.
12. M. J. WHELAN: *Met. Sci.*, 1969, **3**, 95–97.
13. T. HONG, T. DEBROY, S. S. BABU, and S. A. DAVID: *Metall. Mater. Trans.*, 2000, **31B**, 161–169.
14. S. A. COURT and G. POLLARD: *Metallogr.*, 1989, **22**, 219–43.
15. T. HONG and T. DEBROY: *Scr. Mater.*, 2001, **44**, (5), 847–852.
16. G. H. GEIGER and D. R. POIRIER: 'Transport phenomena in metallurgy', 458; 1973, Reading, MA, Addison-Wesley Publishing Co.
17. J. F. ELLIOTT, M. GLEISER, and V. RAMAKRISHNA: 'Thermochemistry for steelmaking', 687–702; 1963, Reading, MA, Addison-Wesley Publishing.
18. E. T. TURKDOGAN: 'Physical chemistry of high temperature technology'; 1980, New York, Academic Press.
19. G. K. SIGWORTH and J. F. ELLIOTT: *Met. Sci.*, 1974, **8**, 298–313.
20. F. D. RICHARDSON: 'Physical chemistry of melts in metallurgy', Vol. 2, 413; 1974, London, Academic Press.
21. J. M. DOWLING, J. M. CORBETT, and H. W. KERR: *Metall. Trans.*, 1986, **17A**, 1611–1623.
22. B. R. KEVILLE: *Weld. J.*, 1983, **62**, (9), 253s–260s.
23. M. WINTZ, M. BOBADILLA, J. LEHMANN, and H. GAYE: *ISIJ Int.*, 1995, **35**, (6), 715–722.